

Ministry of Education and Science of the Russian Federation
FEDERAL STATE-FUNDED EDUCATIONAL
INSTITUTION OF HIGHER EDUCATION
“SAINT PETERSBURG NATIONAL RESEARCH UNIVERSITY OF
INFORMATION TECHNOLOGIES, MECHANICS AND OPTICS”
Faculty of Physics and Engineering

Department of Nanophotonics and Metamaterials

Ang Angeleene

Scattering Forces within a Left-Handed Photonic Crystal

Master’s Thesis

12.04.03 — Nanophotonics and Metamaterials

Admitted for defence.
Head of the chair:
Prof. Pavel Belov

Scientific supervisor:
Dr. Alexander Shalin

Saint-Petersburg
2017

Contents

Introduction	7
1. Optical Forces	12
2. Minimizing Gradient Forces	15
3. Left-Handed Materials	18
4. Forces in LH Materials	21
5. Forces in LPhC structures	25
5.1. Numerical Method	27
5.2. Gajic PhC	28
5.3. Derbali PhC	31
5.4. Foteinopoulou PhC	33
5.5. Guven PhC	35
5.6. Force due to Curl of Spin Density	37
6. Conclusion	39
References	40

Introduction

In Veselago's seminal paper [28], he introduced left-handed (LH) materials - these are defined such that the electric permittivity and the magnetic permeability are simultaneously negative. An effect of LH materials includes an ability to bend light opposite of the conventional way; this phenomenon is known as negative refraction. Additionally, LH materials also have other unusual properties such as subdiffraction focusing, reversed Cherenkov radiation, inversed Doppler effect, reversed Goos–Hanchen shift etc.

Another unusual property of note for LH materials [13] is its capability to produce waves with opposing Poynting vector \mathbf{S} and the electromagnetic momentum \mathbf{p} . Based on this property, this reversed propagation of momentum against the power flow can create negative forces acting on an object inside a left-handed material, and this idea has been discussed in literature [29, 30]. Since the scattering force acting on an object is defined by a change of photon momentum during scattering, this proposition is plausible.

Left-handed material designs were first suggested by Sir Pendry in the year 2000 [14] using a metamaterial composed of nanostructures built from nonmagnetic conducting sheets. To create the effect of negative magnetic permeability, Pendry used an array of split-ring resonators. Possible applications for negative refraction include the creation of perfect flat lenses [20], which could allow imaging below the diffraction limit [25, 1, 2], or modifying signal propagation along transmission lines [7].

However, the existence of negative forces in LH materials remains an open question, since these proposed metamaterials are solid structures, hence preventing any movement of the particles inside.

After the proposal of the first metamaterial designs, left-handed behavior and negative refraction were suggested for photonic crystals (PhC). These are periodic structures that create an environment for photons, analogous to the effects of the usual crystal

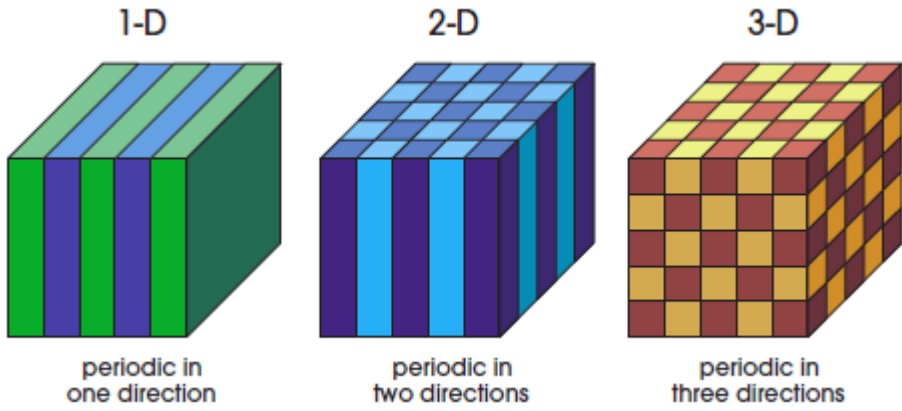


Figure 1. Figure lifted from Joannopoulos [21]. Examples of one, two, and three-dimensional photonic crystals, and the varying colors represent materials with different dielectric constants. The periodicity of the dielectric material is the defining feature of the PhC.

structures for electrons [21]. Using PhCs, we can have control over the propagation of light, much like how semiconductors can manipulate electrons. PhCs can be either one, two, or three-dimensional, as illustrated in Fig. (2).

Analogous to the electronic bandgap, the photonic bandgaps can exist in PhCs for particular frequencies, and these gaps can prevent photon propagation within the crystal structure. For example, a two-dimensional PhC can be used in manipulating the propagation of light inside an optical fiber such that the beam is properly confined inside the structure [23]. One-dimensional PhCs find application in thin-film optics, such as in low and high-reflection coatings in lenses and mirrors [16].

In addition, it was shown that left-handed negative refraction is possible in these structures. With these conditions, the \mathbf{S} and \mathbf{p} vectors can be antiparallel, just like in Veselago's LH materials. PhCs consist of elements larger or comparable in size to the incident wavelength, unlike metamaterials described using an effective medium approach. The empty spaces between the crystal elements are large enough such that one could place particles inside in order to directly test the mechanical action of light. This would allow one to identify how forces behave in a negatively-refracting medium.

The concept of using photonic crystals for manipulating optical forces is also not

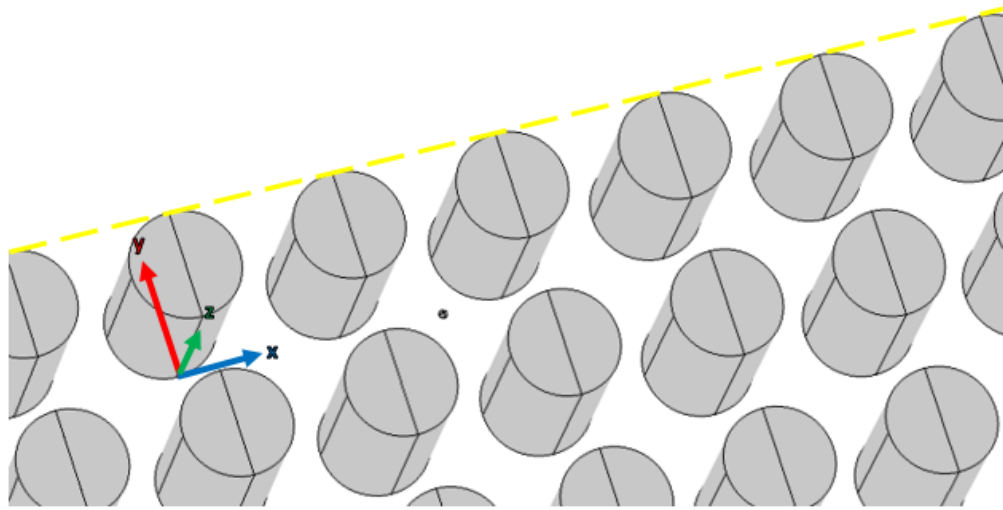


Figure 2. An example structure for a 2D photonic crystal composed of rods. A probe particle has been added in the illustration. The dashed yellow line represents the air-PhC interface; the array of rods extends infinitely both ways in the x and z-directions, infinitely downwards in the y-direction. The rods have been truncated along z-axis here for visual clarity.

new. Previous work has been done to show that calculating forces through a semi-analytical method using the dipolar approximation of the probe particle, as compared to calculating forces through direct integration of the Maxwell stress tensor produces similar results [3], as shown in Fig. (3).

Other methods of generating forces using the properties of photonic crystals to use photonic edge states, and these creates pulling forces. The system, as shown in Fig. (4), is set up such that there is a waveguide where the probe particle is being manipulated.

In this thesis, we use the concept of using left-handed photonic crystals to generate optical forces with the goal of testing the presence of negative forces inside this structure. In addition, while it has been suggested that the composite medium of a PhC can be considered homogeneous [26], we will present an argument that shows otherwise [24].

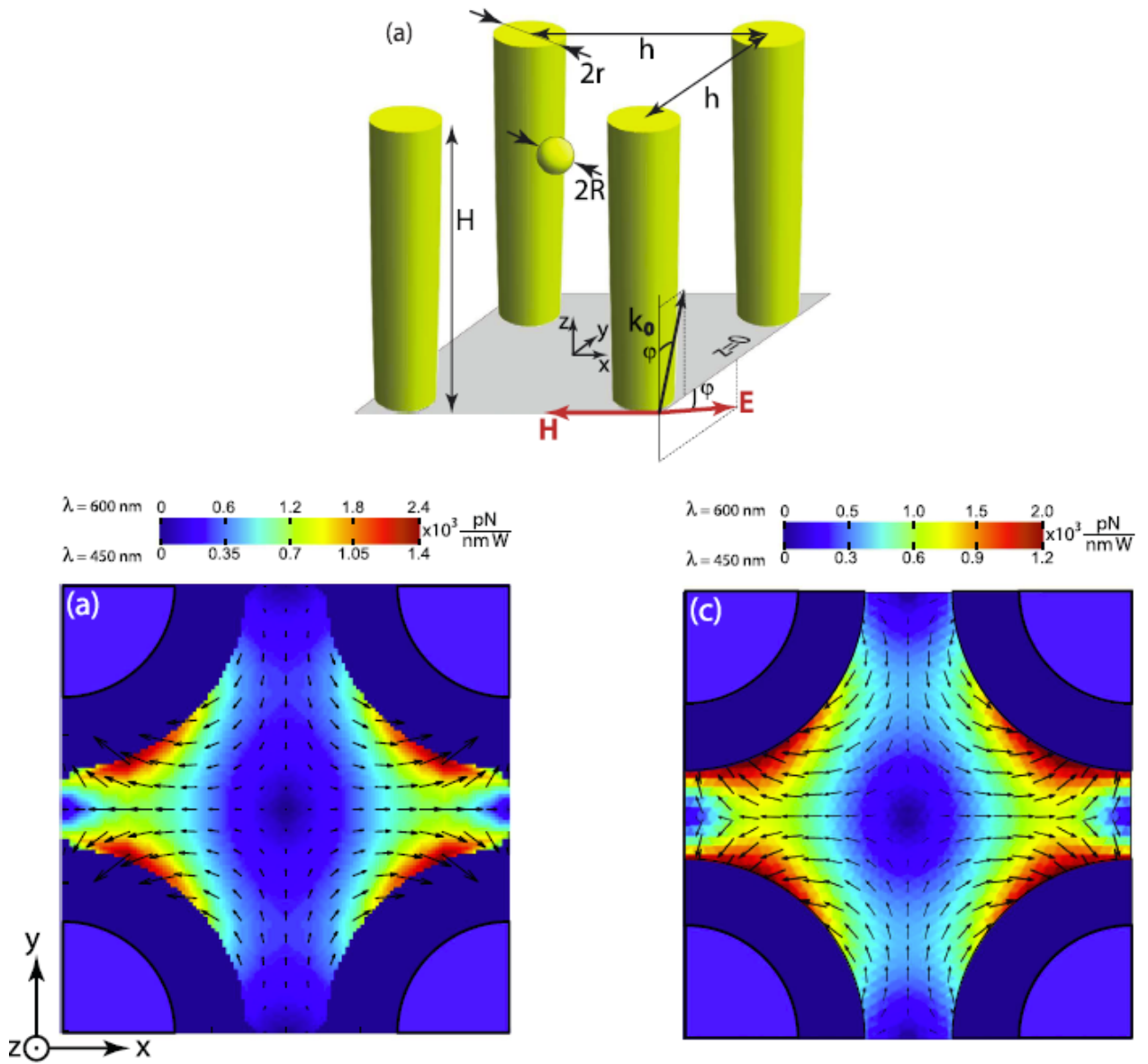


Figure 3. Illustration lifted from the paper of Bogdanov, et al [3]. Figure at the top shows a three-dimensional schematic of their system; the figure at the bottom-left shows the force distribution obtained through integration and the bottom-right shows the force calculated using a semi-analytical approach.

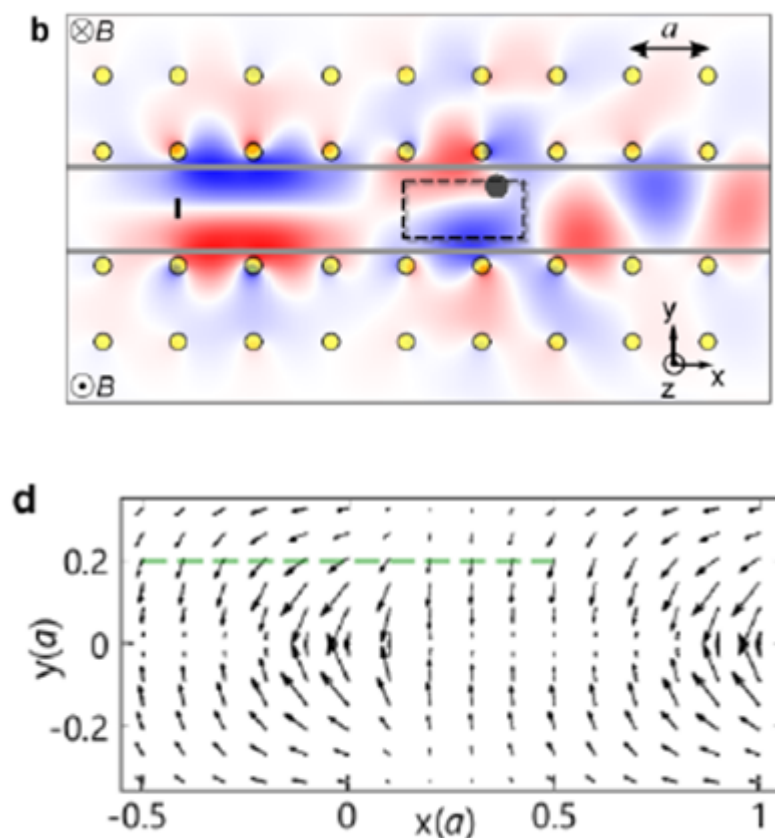


Figure 4. Illustration lifted from the paper of Wang, et al [9]. The system is illustrated at the top figure and the forces are illustrated at the bottom figure. Only the forces in the dashed box of the top figure are shown.

1. Optical Forces

The ability of electromagnetic fields to exert pressure on arbitrary surfaces was first brought up by Kepler to explain why comet tails always point away from the Sun. While the forces due to radiation pressure are usually small in ordinary situations, the resulting forces can be significant in the cases of astrodynamics, and when dealing with objects on the nanoscale. In this section, we present a brief introduction on the mathematics of optical forces.

Starting with the Maxwell Equations in vacuum where

$$\mathbf{D} = \epsilon_0 \mathbf{E} \quad (1a)$$

$$\mathbf{B} = \mu_0 \mathbf{H} \quad (1b)$$

and

$$\nabla \times \mathbf{E} = -\frac{\partial}{\partial t} \mathbf{B} \quad (2a)$$

$$\nabla \times \mathbf{B} = \frac{1}{c^2} \frac{\partial}{\partial t} \mathbf{E} + \mu_0 \mathbf{j} \quad (2b)$$

$$\nabla \cdot \mathbf{E} = -\frac{1}{\epsilon_0} \rho \quad (2c)$$

$$\nabla \cdot \mathbf{B} = 0 \quad (2d)$$

and using the Lorentz force law [11],

$$\mathbf{F} = \int_V [\rho \mathbf{E} + \mathbf{j} \times \mathbf{B}] d\tau \quad (3)$$

where $d\tau$ represents an infinitesimal volume element, for a distribution of charge and currents satisfying the charge conservation law

$$\nabla \cdot \mathbf{j} + \frac{\partial}{\partial t} \rho = 0. \quad (4)$$

Operating on Eq. (2a) by $\times \epsilon_0 \mathbf{E}$ and on Eq. (2b) with Eq. (1b) by $\times \mu_0 \mathbf{H}$ and adding the

two equations, we obtain

$$\nabla \cdot \left[\epsilon_0 \mathbf{EE} - \mu_0 \mathbf{HH} - \frac{1}{2} (\epsilon_0 E^2 + \mu_0 H^2) \overset{\leftrightarrow}{\mathbf{I}} \right] = \frac{d}{dt} \frac{1}{c^2} [\mathbf{E} \times \mathbf{H}] + \rho \mathbf{E} + \mathbf{j} \times \mathbf{B} \quad (5)$$

where the expression at the left is the Maxwell Stress Tensor $\overset{\leftrightarrow}{\mathbf{T}}$ defined as

$$\overset{\leftrightarrow}{\mathbf{T}} = \epsilon_0 \mathbf{EE} - \mu_0 \mathbf{HH} - \frac{1}{2} (\epsilon_0 E^2 + \mu_0 H^2) \overset{\leftrightarrow}{\mathbf{I}}. \quad (6)$$

Taking the divergence of this tensor and integrating over a volume V , this yields

$$\int_V \nabla \cdot \overset{\leftrightarrow}{\mathbf{T}} d\tau = \frac{d}{dt} \frac{1}{c^2} \int_V [\mathbf{E} \times \mathbf{H}] d\tau + \int_V [\rho \mathbf{E} + \mathbf{j} \times \mathbf{B}] d\tau \quad (7)$$

where ρ and \mathbf{j} are the charge and current densities. Using Gauss' law,

$$\int_V \nabla \cdot \overset{\leftrightarrow}{\mathbf{T}} d\tau = \int_{\partial V} \overset{\leftrightarrow}{\mathbf{T}} \cdot \mathbf{n} da \quad (8)$$

in which ∂V is the surface enclosing the volume V , and the vector \mathbf{n} is the vector normal to this surface. At the right hand side of Eq. (7), the two terms are the field and mechanical momentum,

$$\mathbf{G}_{field} = \frac{1}{c^2} \int_V [\mathbf{E} \times \mathbf{H}] d\tau \quad (9a)$$

$$\frac{d}{dt} \mathbf{G}_{mech} = \int_V [\rho \mathbf{E} + \mathbf{j} \times \mathbf{B}] d\tau \quad (9b)$$

The field momentum is zero when averaged over one oscillation period, and the average mechanical force is given by [17, 19],

$$\langle \mathbf{F} \rangle = \int_{\partial V} \langle \overset{\leftrightarrow}{\mathbf{T}}(\mathbf{r}, t) \rangle \cdot \mathbf{n}(\mathbf{r}) da, \quad (10)$$

where $\langle \dots \rangle$ indicates the time average. While the force expression is not dependent on the material properties, we note that it is needed for the material to be rigid. If we have a deformable body due to an electromagnetic field, we also have to include the forces due to the electrostrictive and magnetostrictive forces.

In order to obtain the electromagnetic force acting on a dipolar particle, we consider a particle having both electric and magnetic dipole moments, separated by a small distance \mathbf{s} and illuminated an arbitrary electromagnetic field. Expressing the field through the Taylor expansion, the time-averaged force acting on the system of particles becomes [19]

$$F_x = \frac{1}{2} \operatorname{Re} \left[\alpha_e E_j \frac{\partial E_j^*}{\partial x} \right] + \frac{1}{2} \operatorname{Re} \left[\alpha_m H_j \frac{\partial H_j^*}{\partial x} \right] - \frac{k^4}{12\pi\epsilon_0 c} \operatorname{Re} [\epsilon_{ijk} \alpha_e E_j (\alpha_m H_k)^*] \quad (11)$$

for the x-component of the force, and ϵ_{ijk} is the Levi-Civita tensor. The first term in the expression is the force due to the electric dipole moment of the probe particle, the second is due to the magnetic dipole moment, and the third is due to the interaction of the electric and dipole moments. There exist forces for the higher-order terms of the probe particle [19], but in this thesis, we consider only the first term in this equation.

The first term in Eq. (11) can be written as

$$\langle \mathbf{F} \rangle = \frac{\alpha'}{4} \nabla \langle |\mathbf{E}|^2 \rangle + \frac{\alpha''}{2} \langle |\mathbf{E}|^2 \rangle \nabla \phi \quad (12)$$

and in this equation, ϕ is the phase of the field, and $\alpha = \alpha' + i\alpha''$ is the real and imaginary parts of the particle polarizability, respectively.

The first term in Eq. (12), proportional to the real part of the particle polarizability, corresponds to the conservative (non-solenoidal) gradient force. The second term, proportional to the imaginary parts of the polarizability, corresponds to the non-conservative scattering force. We are particularly interested in the second term, as this allows unrestricted particle motion.

2. Minimizing Gradient Forces

For our task, we want to minimize the gradient forces; these are responsible for the trapping of particles in high-intensity locations of the electric field. The effect of trapping, while useful in other applications, is undesirable for our purposes, as we are investigating the existence of negative forces. Hence, we want to use a particle whose imaginary polarizability is larger than the real part.

Considering a spherical particle, the polarizability [6] can be obtained through the Clausius-Mossotti relation

$$\alpha = 4\pi r^3 \epsilon_0 \frac{\epsilon_p - \epsilon_a}{\epsilon_p + 2\epsilon_a}, \quad (13)$$

where the complex permittivity is given as

$$\epsilon_p = \epsilon'_p + i\epsilon''_p. \quad (14)$$

Equation (13) should also have radiative correction [6] $k^3 a$, but in the case of complex permeability, the correction is small and can be omitted. The polarizability can be separated into real and imaginary parts, as follows

$$\alpha = 4\pi r^3 \epsilon_0 \left[\frac{(\epsilon'_p)^2 + (\epsilon''_p)^2 - 2\epsilon_a^2 + \epsilon_a \epsilon'_p}{(\epsilon'_p + 2\epsilon_a)^2 + (\epsilon''_p)^2} + i \frac{3\epsilon_a \epsilon''_p}{(\epsilon'_p + 2\epsilon_a)^2 + (\epsilon''_p)^2} \right]. \quad (15)$$

Ideally, we want the real part of α to be only zero, as this would mean that the probe particle would only be affected by the nonconservative optical force. For our case,

$$\epsilon_a \epsilon''_p \neq 0. \quad (16)$$

In addition, we need to find ϵ_p such that

$$\text{Re}(\alpha) = 4\pi r^3 \epsilon_0 \frac{(\epsilon'_p)^2 + (\epsilon''_p)^2 - 2\epsilon_a^2 + \epsilon_a \epsilon'_p}{(\epsilon'_p + 2\epsilon_a)^2 + (\epsilon''_p)^2} = 0 \quad (17)$$

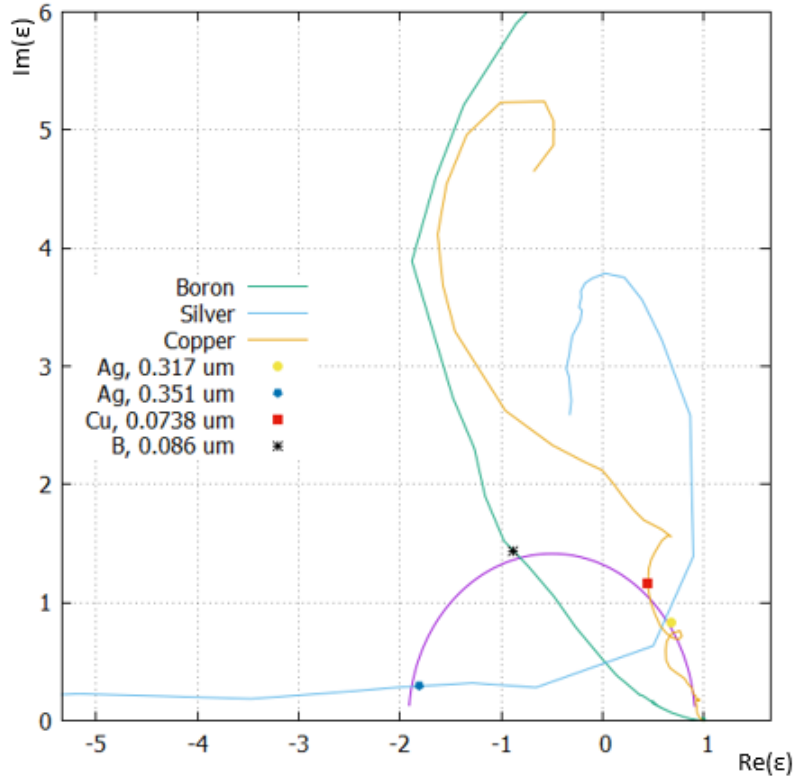


Figure 5. Plot of the real part of dielectric permittivity versus its imaginary part with a locus of points (purple half-circle) specifying zero real part of polarizability of the probe particle (Eq. (19)). The points indicate the permittivities for zero real polarizability

and from this, we obtain

$$\epsilon'_p = \pm \sqrt{\frac{9}{4}\epsilon_a^2 - (\epsilon''_p)^2} - \frac{1}{2}\epsilon_a \quad (18)$$

Combining this and Eq. (14), we obtain the following condition:

$$\epsilon_p = \pm \sqrt{\frac{9}{4}\epsilon_a^2 - \epsilon''_p^2} - \frac{1}{2}\epsilon_a + i\epsilon''_p \quad \text{and} \quad 0 < \epsilon''_p \leq \frac{3}{2}\epsilon_a \quad (19)$$

Equation (19) can be visualized in a parametric plot with the real polarizability in the x-axis, the imaginary part in the y-axis, and the plot parameter is the incident frequency. If the material's plot intersects the half-circle (see Fig. (5)), the material at that parameter (frequency) can be used for minimizing the gradient force.

If we were to consider materials in air composed of only element, the minimized gradient condition in Eq. (19) is satisfied by Silver [12] - the point (0.679, 0.825) in Fig. (5)

corresponds to $\lambda = 0.317 \mu m$ wavelength and the point $(-1.814, 0.297)$ corresponds to $\lambda = 0.351 \mu m$, Boron [18] - the point $(-0.888, 1.439)$ corresponds to $\lambda = 0.086 \mu m$, and Copper [10] - the point $(0.447, 1.16)$ corresponds to $\lambda = 0.074 \mu m$. In addition, the condition is satisfied by Gold nanoparticles submerged in a liquid with high refractive index [15, 4]. It is also possible to consider probe particles that are made of composite materials to bring the wavelength in the visible range.

3. Left-Handed Materials

Veselago, in his seminal paper [28], proposed a theoretical material in which the Poynting vector and the propagation of the wave propagation are opposite each other. As mentioned in the introduction, these materials and their unusual properties have many applications. For this section, we show how opposing Poynting and propagation vectors arises from simultaneously negative permeability and permittivity.

The values of the dielectric constant ϵ and the magnetic permeability μ are the fundamental characteristic quantities which determine the propagation of electromagnetic waves in matter, as they are the only material parameters which appears in the dispersion equation

$$k^2 = \frac{\omega^2}{c^2} n^2 = \frac{\omega^2}{c^2} \epsilon \mu. \quad (20)$$

If we only look at no-loss materials (i.e., n , ϵ and μ are only real-valued), then we note that Eq. (20) does not change if both ϵ and μ have simultaneously negative values.

We consider the Maxwell equations Eqns. (2b and 2a) in matter with no free current along with Eqns. (1b and 1a). For a monochromatic plane wave, where all quantities are proportional to $e^{i(kz-\omega t)}$, the expressions in the Maxwell Equations reduce to

$$\mathbf{k} \times \mathbf{E} = \omega \mu \mathbf{H} \quad (21a)$$

$$\mathbf{k} \times \mathbf{H} = -\omega \epsilon \mathbf{E} \quad (21b)$$

From these set of equations, we can see that if $\epsilon > 0$ and $\mu > 0$, then \mathbf{E} , \mathbf{H} , and \mathbf{k} form a right-handed set of vectors. On the other hand, if $\epsilon < 0$ and $\mu < 0$, then the vectors form a left-handed vector set.

The direction of the power flow carried by the electromagnetic wave is determined by the Poynting vector \mathbf{S} , defined as

$$\mathbf{S} = \mathbf{E} \times \mathbf{H} \quad (22)$$

From the definition of the vector product, the Poynting vector always follows a right-handed set with the electric and magnetic fields. Similarly, for right-handed substances, the Poynting vector and the direction of wave propagation \mathbf{k} are in the same direction. On the other hand, for left-handed materials, these two vectors are in opposite directions.

It is also important to note that positive refraction can still happen with left-handed beams, and positive phase velocity can occur in negatively-refracting fields. This is illustrated in Fig. (6).

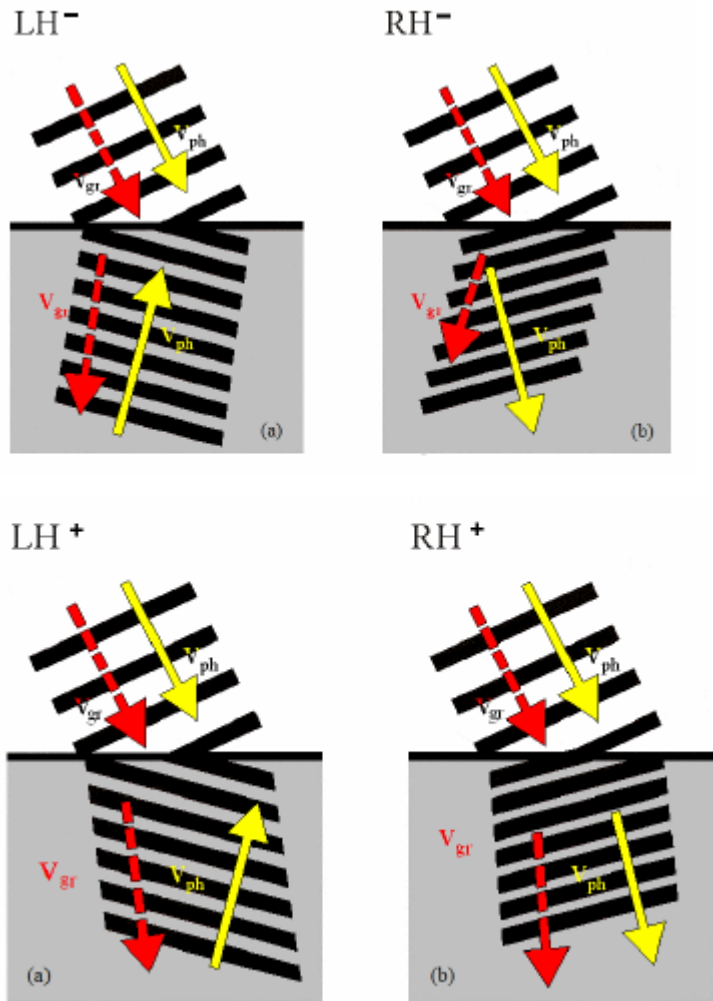


Figure 6. Figure lifted from the paper of Gajic [22]. The plus and minus signs indicate positive and negative refraction, respectively. "LH" and "RH" respectively signify the left-handedness and right-handedness.

4. Forces in LH Materials

If we were to look at the forces inside a homogeneous left-handed structure with simultaneously negative permittivity and permeability, we obtain the force field in Fig. (7). This proves our initial hypothesis – since the power flow and forces would be in opposite directions inside the left-handed material, and the power flow would only go downwards, then negative forces would arise such a material.

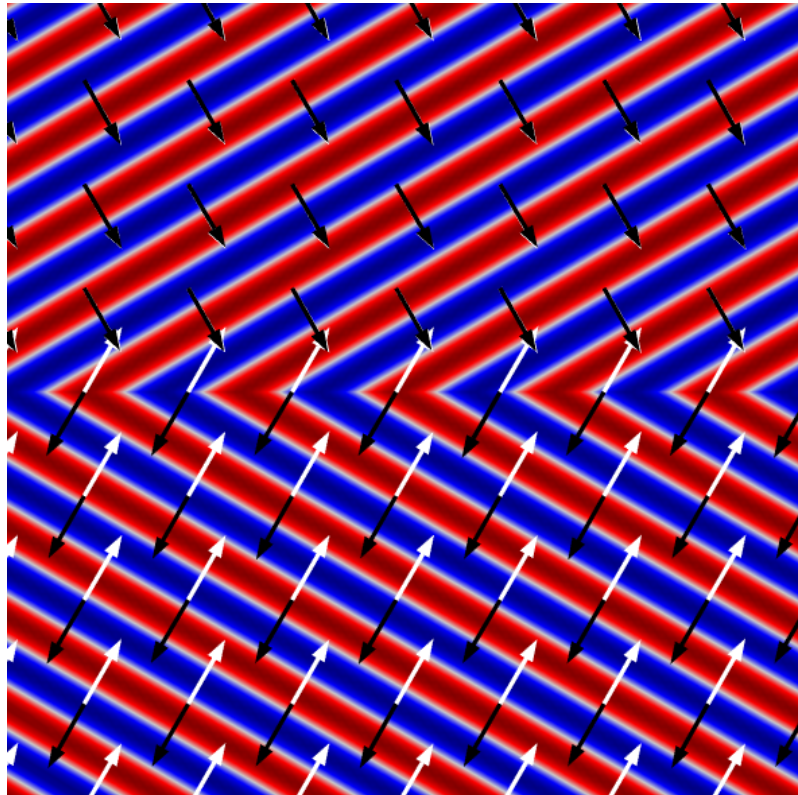


Figure 7. The forces and power flow in a homogeneous left-handed material with $\epsilon = \mu = -1$, derived using the first term of Eq. (11). The color map represents the H-field, the black arrows represent the power flow, and the white arrows represent the forces. The upper half of the figure has parameters $\epsilon = \mu = 1$, and the force arrows coincide directly with the power flow arrows.

However, in a realistic application, we cannot use a homogeneous material as the background where our probe particle can be manipulated. This is because our proposed homogeneous material is a solid, and the object cannot move inside such material.

We further note the decomposition of the scattering force in Eq. (12), which can be

obtained using vector identities:

Starting with

$$\langle F_x \rangle = \frac{1}{2} \operatorname{Re} \left(\alpha \mathbf{E} \cdot \frac{\partial \mathbf{E}^*}{\partial x} \right) \quad (23)$$

using the vector identity

$$\nabla_{\mathbf{x}} (\mathbf{y} \cdot \mathbf{x}) = \mathbf{y} \times (\nabla \times \mathbf{x}) + (\mathbf{y} \cdot \nabla) \mathbf{x} \quad (24)$$

where $\nabla_{\mathbf{x}}$ indicates that the ∇ operator only acts on \mathbf{x} , then the force vector can be written as

$$\langle \mathbf{F} \rangle = \frac{1}{2} \operatorname{Re} (\alpha [\mathbf{E} \cdot \nabla] \mathbf{E}^* + \alpha [\mathbf{E} \times (\nabla \times \mathbf{E}^*)]). \quad (25)$$

From linearity,

$$\langle \mathbf{F} \rangle = \frac{1}{2} \operatorname{Re} (\alpha [\mathbf{E} \cdot \nabla] \mathbf{E}^*) + \frac{1}{2} \operatorname{Re} (\alpha [\mathbf{E} \times (\nabla \times \mathbf{E}^*)]) \quad (26)$$

The first term here can be rewritten using the complex number identities

$$\operatorname{Re}(ab) = \operatorname{Re}(a)\operatorname{Re}(b) - \operatorname{Im}(a)\operatorname{Im}(b) \quad (27a)$$

$$\operatorname{Im}(a) = -\operatorname{Re}(i \cdot a) \quad (27b)$$

$$\operatorname{Re}(a) = \frac{1}{2} (a + a^*) \quad (27c)$$

$$\operatorname{Im}(a) = \frac{1}{2i} (a - a^*) \quad (27d)$$

so that we can obtain

$$\operatorname{Re} (\alpha [\mathbf{E} \cdot \nabla] \mathbf{E}^*) = \operatorname{Re}(\alpha) \operatorname{Re} ([\mathbf{E} \cdot \nabla] \mathbf{E}^*) + \operatorname{Im}(\alpha) \operatorname{Re} (i [\mathbf{E} \cdot \nabla] \mathbf{E}^*) \quad (28)$$

and subsequently,

$$\operatorname{Re} ([\mathbf{E} \cdot \nabla] \mathbf{E}^*) = \frac{1}{2} [(\mathbf{E} \cdot \nabla) \mathbf{E}^* + (\mathbf{E}^* \cdot \nabla) \mathbf{E}]. \quad (29)$$

The term inside the brackets can be simplified through this identity

$$\nabla(\mathbf{x} \cdot \mathbf{y}) = (\mathbf{x} \cdot \nabla)\mathbf{y} + (\mathbf{y} \cdot \nabla)\mathbf{x} + \mathbf{x} \times (\nabla \times \mathbf{y}) + \mathbf{y} \times (\nabla \times \mathbf{x}) \quad (30)$$

hence

$$\operatorname{Re}([\mathbf{E} \cdot \nabla] \mathbf{E}^*) = \frac{1}{2} [\nabla(|\mathbf{E}|^2) - \mathbf{E} \times (\nabla \times \mathbf{E}^*) - \mathbf{E}^* \times (\nabla \times \mathbf{E})] \quad (31)$$

However, in the second term of Eq. (26), we have a term which can be expanded, as follows:

$$\operatorname{Re}(\alpha [\mathbf{E} \times (\nabla \times \mathbf{E}^*)]) = \operatorname{Re}(\alpha) \operatorname{Re}(\mathbf{E} \times [\nabla \times \mathbf{E}^*]) - \operatorname{Im}(\alpha) \operatorname{Im}(\mathbf{E} \times [\nabla \times \mathbf{E}^*]) \quad (32)$$

and we note that

$$\operatorname{Re}(\mathbf{E} \times [\nabla \times \mathbf{E}^*]) = \frac{1}{2} \{(\mathbf{E} \times [\nabla \times \mathbf{E}^*]) + (\mathbf{E}^* \times [\nabla \times \mathbf{E}])\}. \quad (33)$$

Combining these equations together, the force can now be written as

$$\langle \mathbf{F} \rangle = \frac{1}{4} \operatorname{Re}(\alpha) \nabla |\mathbf{E}|^2 + \frac{1}{2} \operatorname{Im}(\alpha) \operatorname{Re}(i [\mathbf{E} \cdot \nabla] \mathbf{E}^*) - \frac{1}{2} \operatorname{Im}(\alpha) \operatorname{Im}(\mathbf{E} \times [\nabla \times \mathbf{E}^*]). \quad (34)$$

If we use the Maxwell's equation with time-harmonic fields, we have $\nabla \times \mathbf{E} = i\omega\mu_0\mathbf{H}$. We then obtain

$$\langle \mathbf{F} \rangle = \frac{1}{4} \operatorname{Re}(\alpha) \nabla |\mathbf{E}|^2 - \frac{1}{2} \operatorname{Im}(\alpha) \operatorname{Im}([\mathbf{E} \cdot \nabla] \mathbf{E}^*) + \omega\mu_0 \frac{1}{2} \operatorname{Im}(\alpha) \operatorname{Re}(\mathbf{E} \times \mathbf{H}^*). \quad (35)$$

The second term of Eq. (35) can be expanded as

$$\operatorname{Im}([\mathbf{E} \cdot \nabla] \mathbf{E}^*) = \frac{1}{2i} \{([\mathbf{E} \cdot \nabla] \mathbf{E}^*) - ([\mathbf{E}^* \cdot \nabla] \mathbf{E})\}, \quad (36)$$

and using the following vector identity

$$\nabla \times (\mathbf{x} \times \mathbf{y}^*) = \mathbf{x} (\nabla \cdot \mathbf{y}) - \mathbf{y} (\nabla \cdot \mathbf{x}) + (\mathbf{y} \cdot \nabla) \mathbf{x} - (\mathbf{x} \cdot \nabla) \mathbf{y} \quad (37)$$

where we note that $\nabla \cdot \mathbf{E} = 0$ in our case, then Eq. (35) becomes

$$\langle \mathbf{F} \rangle = \frac{1}{4} \operatorname{Re}(\alpha) \nabla |\mathbf{E}|^2 + \frac{1}{4i} \operatorname{Im}(\alpha) \nabla \times (\mathbf{E} \times \mathbf{E}^*) + \omega \mu_0 \frac{1}{2} \operatorname{Im}(\alpha) \operatorname{Re}(\mathbf{E} \times \mathbf{H}^*). \quad (38)$$

We write the time-averaged Poynting vector as

$$\langle \mathbf{S} \rangle = \frac{1}{2} \operatorname{Re}[\mathbf{E} \times \mathbf{H}^*], \quad (39)$$

the total cross section of a dipolar particle as

$$\sigma = \frac{k}{\epsilon_0} \operatorname{Im}(\alpha), \quad (40)$$

and the spin angular momentum of the field as

$$\langle \mathbf{L}_s \rangle = \frac{1}{4\omega i} \epsilon_0 [\mathbf{E} \times \mathbf{E}^*], \quad (41)$$

we finally obtain

$$\langle \mathbf{F} \rangle = \frac{1}{4} \operatorname{Re}(\alpha) \nabla |\mathbf{E}_0|^2 + \sigma \frac{1}{c} \langle \mathbf{S} \rangle + \sigma c \nabla \times \langle \mathbf{L}_s \rangle \quad (42)$$

The scattering force decomposes into the force in the direction of the Poynting vector, and the force due to the curl of the spin density of the transverse electromagnetic field.

5. Forces in LHPHc structures

In a previous section, we note that we have a specific frequency at which we want the incident field to have. At the same time, negative refraction arises in particular photonic crystals only in particular frequencies. Luckily, these crystal structures are scalable, meaning that we can change the frequency of the incident field, and we obtain the same effects as long as we properly change the crystal parameters. We do this through the use of the normalized frequency defined as the \tilde{f} , and the fill ratio.

The system which we consider is illustrated in Fig. (8).

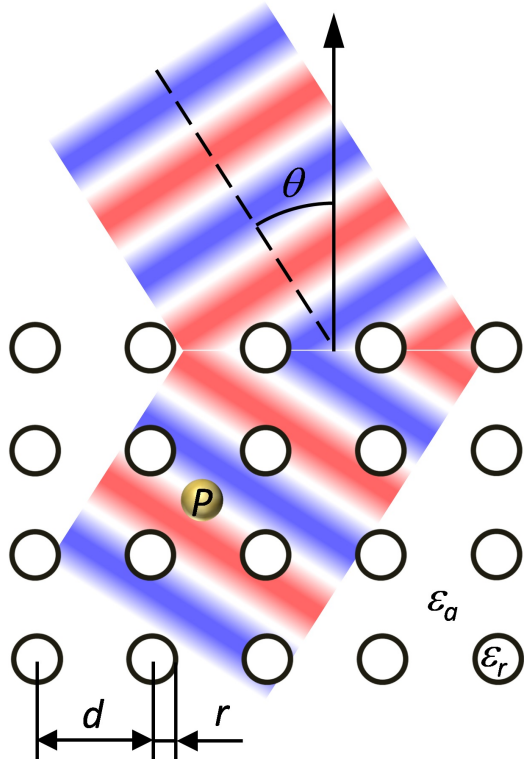


Figure 8. The geometry of our system - an external wave is incident at an angle θ onto the surface of a left-handed photonic crystal. The dipolar particle P serves as the probe for the local optical forces.

Additionally, we need crystals such that the individual rods have enough space between them, so that the particle can move. This gap is characterized by the crystal's fill ratio, the fraction of the rod radius and the distance between the rods. A fill ratio of 0.5 indicates the individual rods in contact with the next rod, and this would be un-

acceptable for our purposes. Given these considerations, we use four two-dimensional photonic crystals – two of which have square lattices, and the other two with triangular lattices - and all these four crystals have previously shown negative refraction in their respective papers.

Table 1. A list of the photonic crystals demonstrating negative refractive index. For all cases, the permittivity of the host material ϵ_a is unity.

Reference	Lattice	fill, r/d	ϵ_r	θ	$\tilde{f} = fd/c$
[22]	square	0.33	9.61	15°	0.413
[5]	square	0.22	8.9	10°	0.732
[8]	triangular	0.35	12.96	30°	0.58
[27]	triangular	0.329	9.61	30°	0.667

Also, we note that the third term in the force given by the expression in Eq. (42) is zero in the case of crystals with TM-polarized incident fields, where the E-field is parallel to the rod axis. Therefore, in this thesis, we consider only incident fields in which the H-field is parallel to the rod axes, referred to as TE-polarization. In the case of incident TM-polarization, the spin angular momentum in Eq. (41) becomes zero and the scattering force would go in the direction of the Poynting vector. However, the Poynting vector cannot move up the crystal structure, hence we can already conclude that negative forces cannot exist in PhCs with incident TM-polarizationn.

5.1. Numerical Method

The calculation of the electromagnetic fields inside the four 2D PhCs were performed using finite-elements method in COMSOL Multiphysics 5.1.

Initially, one unit cell of the PhC is made using the parameters in Table 1, then this is copied ten times in the vertical direction to simulate an infinite or very long photonic crystal in that direction. Additionally, to prevent wave reflection from the bottom of the crystal, a dielectric loss of 0.05 was included to the permittivity of the rods. For the left and right edges, periodic boundary conditions were set at those locations of the simulation domain, such that the system will appear infinite.

For the mesh settings, the left and right meshes were set up such that they are identical. For the top and bottom edges, we used periodic ports, in which the top edge is providing the excitation for the plane wave. A free triangular mesh with minimum element size $\lambda/10/\sqrt{|\epsilon_r|}$ was used for the entire domain.

Lastly, the variables for the forces were assigned in COMSOL using the first term of Eq. (11). The separated conservative and nonconservative force components were calculating using Eq. (42), and we confirmed that the forces using the first term of Eq. (11) and the sum of the terms in Eq. (42) are identical.

5.2. Gajic PhC

The first structure that we will consider is from the paper of Gajic, Meisels, et al [22]. Their original left-handed structure is made of Al_2O_3 rods with fill ratio 0.33 and an incident field with frequency of 67 GHz and refractive index 3.1. The incident field is at a 15° angle.

In this crystal structure, we see the power flow moving in circles around specific locations in the unit cell, in Fig. (10). While some points in the domain have upward-moving power flow, the overall power flow goes in the downward direction. We notice in Fig. (10) that the force field does not follow the energy flow. This is caused by the nonzero spin density term in Eq. (42). While the optical force goes away from the location of the interface, and the force also moves to the left corresponding to negative refraction, the force is not negative.

In addition, we also performed a simulation of this photonic crystal using a three-dimensional simulation consisting of rods. The result is shown in Fig. (11), and comparing this to the forces in Fig. (10, right), we confirm that the forces are the same if we use either the semi-analytical approach using the dipole approximation, or if we integrate the Maxwell stress tensor around the probe particle.

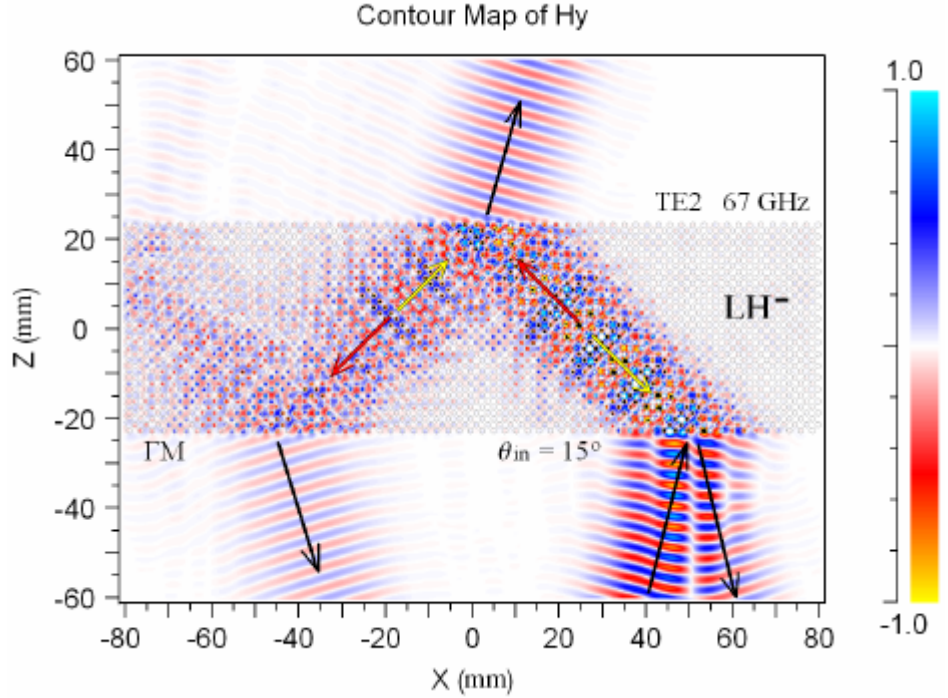


Figure 9. Original figure shown in the paper of Gajic [22]. The backward movement of the phase velocity is shown in a video supplementary to the original paper, and the phase (yellow) and group (red) velocities are illustrated in this figure.

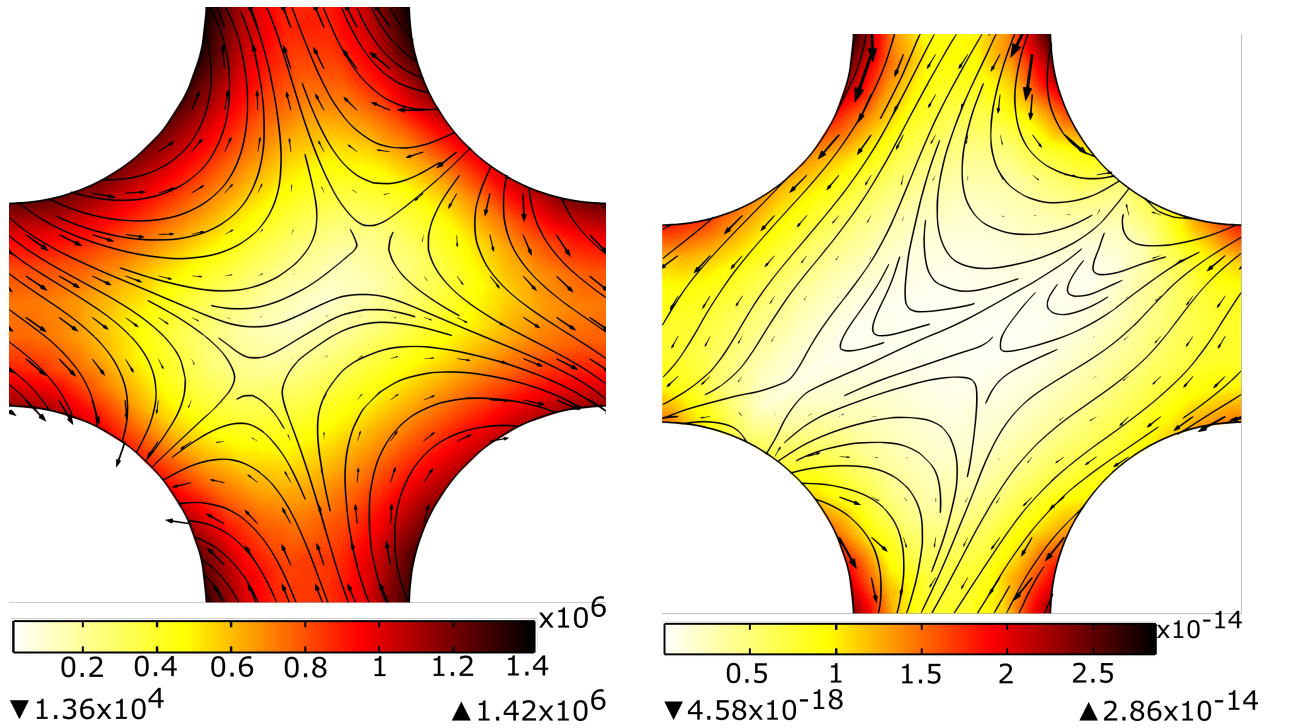


Figure 10. A unit cell of the PhC with parameters taken from Ref. [22]. The figure at the left shows the plot of the electric field amplitude (color map) and power flow (arrows), while the right shows the optical force magnitude (color map), direction (arrows), and possible trajectories (lines) for the probe particle. The interior of the rods is not shown.

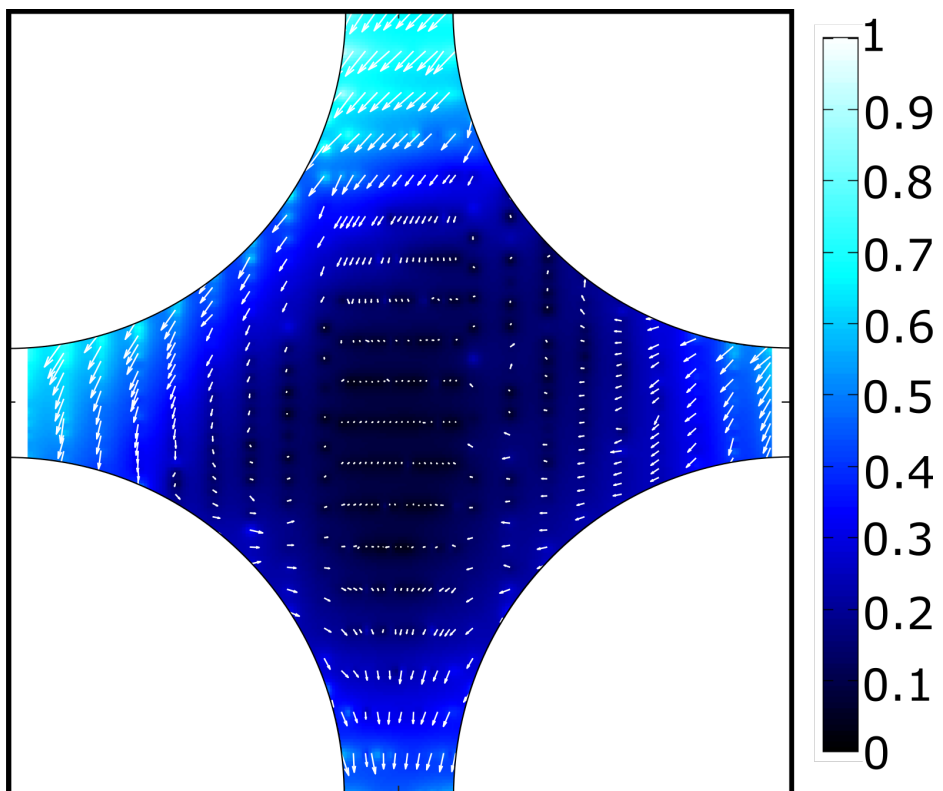


Figure 11. Normalized force inside the PhC unit cell of Gajic [22] obtained through integration of the Maxwell Stress Tensor. The color map shows the force magnitude and the arrows show the direction of the force.

5.3. Derbali PhC

Our second structure comes from the paper of Derbali and AbdelMalek [5]. Similar to Gajic's paper, they used a square lattice, but their fill ratio is smaller, hence producing larger spaces between the rods, and their rods are made of Aluminum with dielectric constant $\epsilon = 8.9$. The fill ratio of the crystal system is given as 0.22, the normalized frequency is 0.732, and the beam is incident at an angle of 10° .

The result in their paper showed dual self-collimation for a 2D photonic crystal with a thickness of six rods. Negative phase velocity was outside the scope of their paper and was not shown. In this crystal structure, we see that the forces and power flow, shown in Fig. (12) do not go in the exact same direction. While the forces are "negatively-refracting", they are still moving in the positive direction (away from the interface).

One thing this force simulation does not have in common with Fig. (10) is that there are maxima of the E-field amplitude does not correspond to a maxima of the force magnitude, as shown by the top-right and bottom-left rods in Fig. (12), whereas the maxima of the E-field amplitude corresponds to the maxima of the forces in Fig. (10).

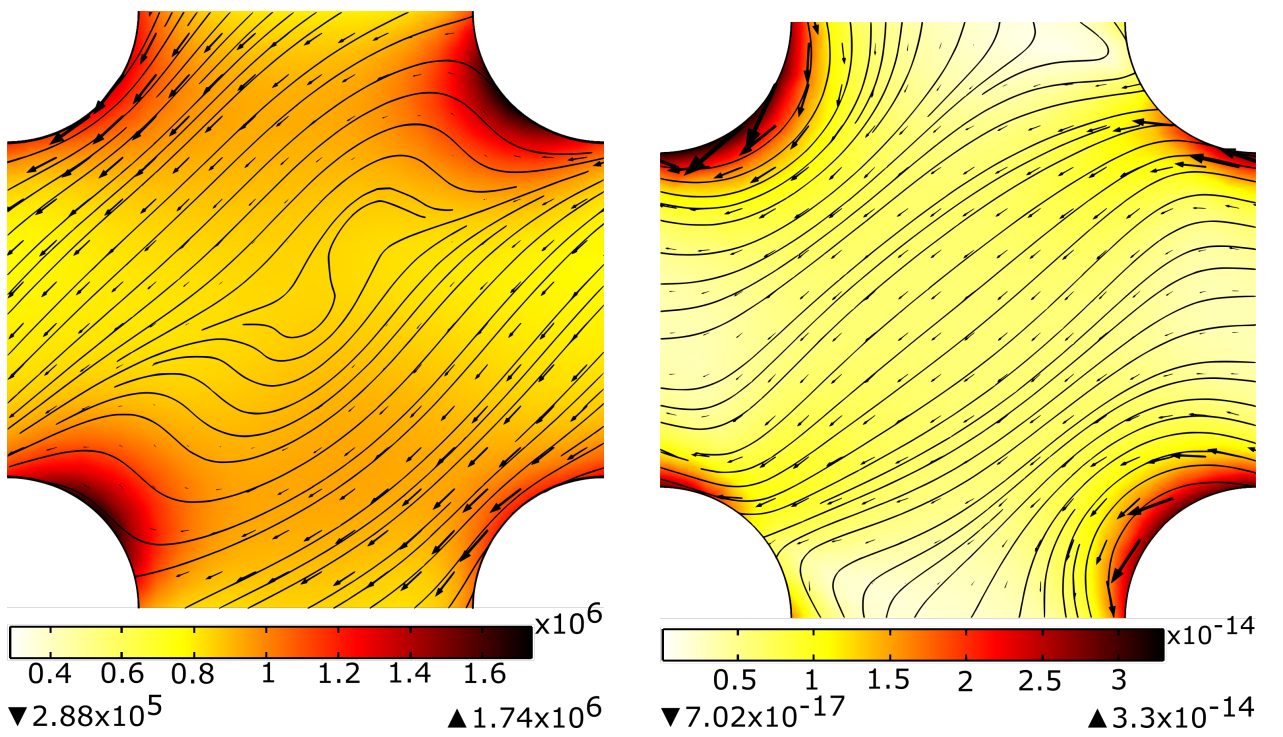


Figure 12. A unit cell of the PhC with parameters taken from Ref. [5]. The figure at the left shows the plot of the electric field amplitude (color map) and power flow (arrows), while the right shows the optical force magnitude (color map), direction (arrows), and possible trajectories (lines) for the probe particle. The interior of the rods is not shown.

5.4. Foteinopoulou PhC

The next structure taken from the paper of Foteinopoulou, et al. [8] uses a hexagonal/triangular lattice of rods with dielectric constant $\epsilon = 12.96$, radius of $r = 0.35a$, and a is the lattice constant of the system. The incident angle used in the simulation is 30° . The field incident used in the simulation has a dimensionless frequency of 0.58, but their paper showed that negative refraction and negative phase velocity is possible for frequencies between 0.57 and 0.61.

In this simulation - results shown in Fig. (13), similar to the previous figures, we see that the force does not go in the direction of the power flow. Here, we see that changing the lattice of the photonic crystal also does not produce negative forces inside the crystal structure, though we do see that the forces appear to be in a "negatively refracting" direction.

Similar to Fig. (12), the E-field maxima in Fig. (13) does not appear to correspond to the maxima of the forces. The location with maximum force magnitudes appear to be the minima of the E-field amplitude near the rods instead. Additionally, there exists E-field maxima in the spaces between the rods where the force magnitude appears to be minimized.

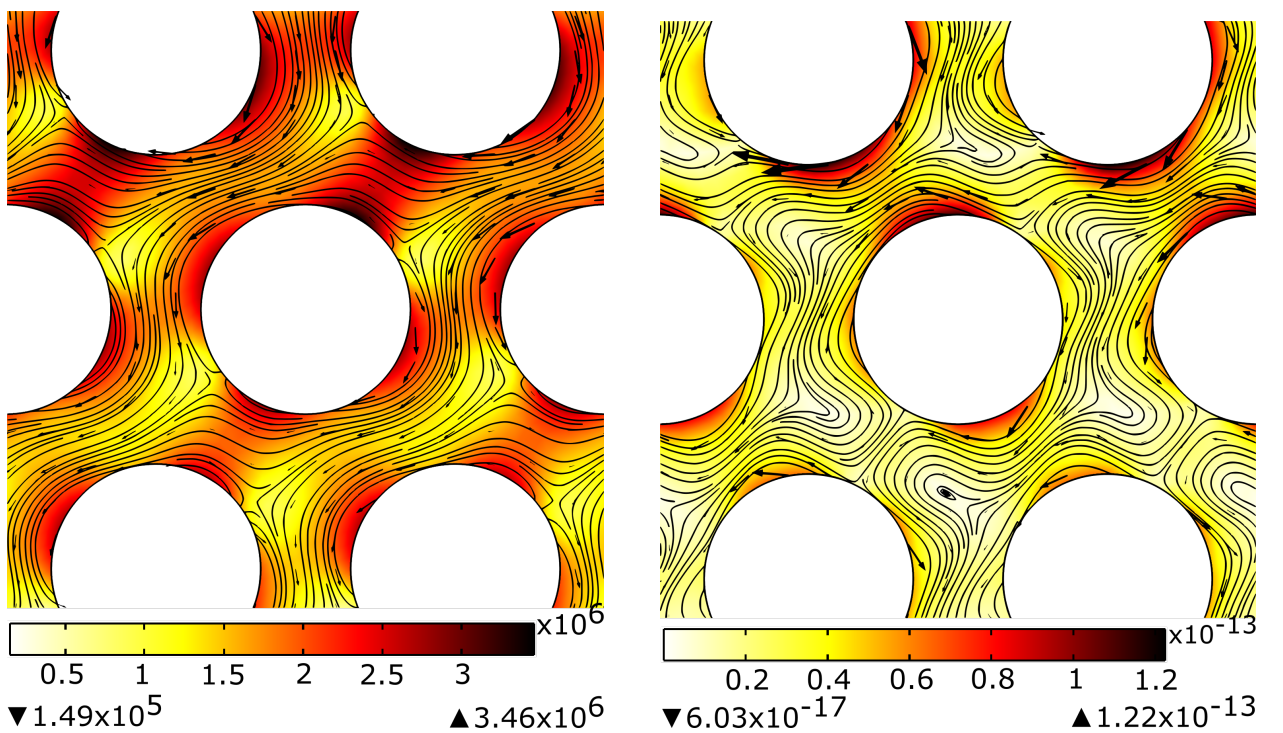


Figure 13. A unit cell of the PhC with parameters taken from Ref. [8]. The figure at the left shows the plot of the electric field amplitude (color map) and power flow (arrows), while the right shows the optical force magnitude (color map), direction (arrows), and possible trajectories (lines) for the probe particle. The interior of the rods is not shown.

5.5. Guven PhC

The fourth structure in this thesis comes from the paper of Guven, Aydin, et al. [27] In their paper, they were able to experimentally show negative refraction in a hexagonal/triangular photonic crystal, and used this property in order to show the ability of a flat photonic crystal slab to focus an incident field. Their crystal is composed of aluminum rods with dielectric constant $\epsilon = 9.61$, with lattice period $a = 4.79$ mm, diameter $2r = 3.15$ mm, and the original incident frequency used is $f = 41.7$ GHz. The paper shows that three angles - 15° , 30° , and 45° - show negative refraction in both simulation and experiment. In our simulation, we used an incident field of 30° .

This simulation uses a different material for the rods, and here we see in Fig. (14) that changing the material also does not produce negative forces. Similar to the previous results, the radiation pressure remains positive, and the movement of the force goes in a negatively refracting direction. If we are to compare the relationship of the E-field maxima and the force maxima, it again does not correspond with each other. The force maxima appears to be along a particular diagonal line connecting the rods, and this pattern is does not appear in the E-field maxima plot.

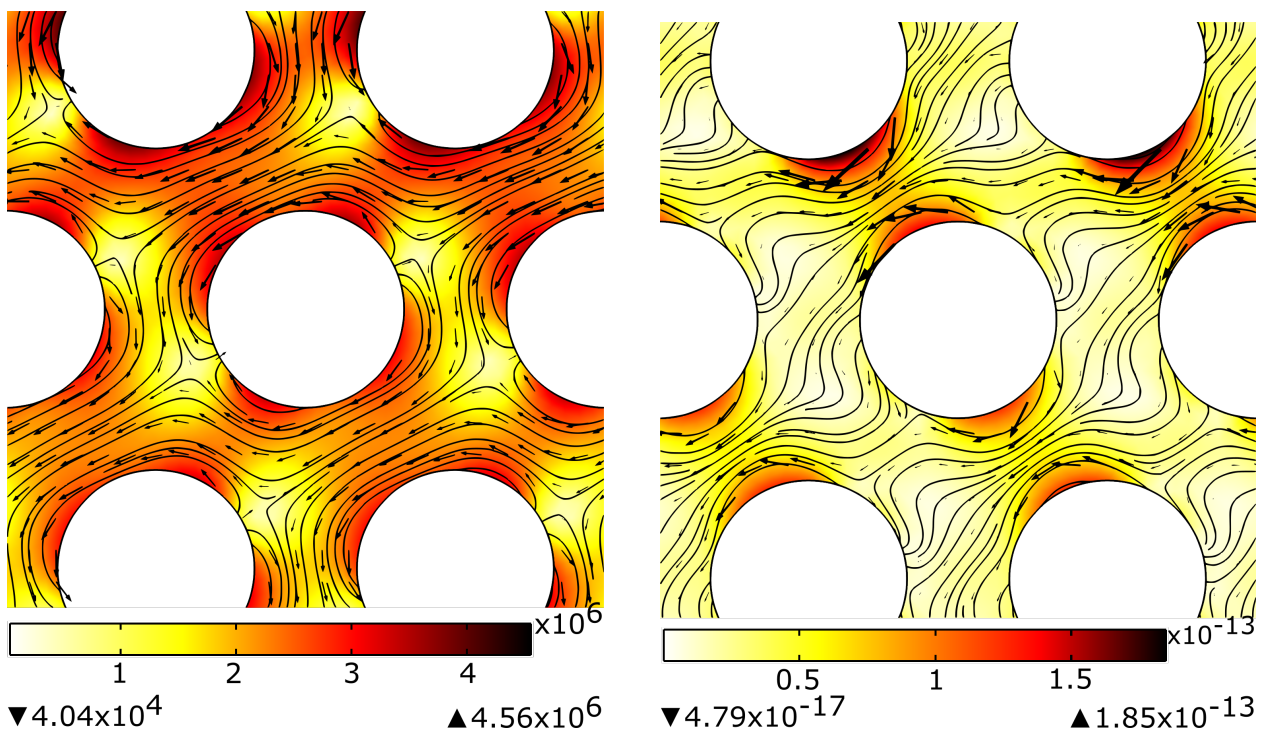


Figure 14. A unit cell of the PhC with parameters taken from Ref. [27]. The figure at the left shows the plot of the electric field amplitude (color map) and power flow (arrows), while the right shows the optical force magnitude (color map), direction (arrows), and possible trajectories (lines) for the probe particle. The interior of the rods is not shown.

5.6. Force due to Curl of Spin Density

Since we already know that the term of the optical force which goes in the direction of the Poynting vector will only go in the positive direction, we can look at the other term of the scattering force, the term which is proportional to the curl of the spin density.

The simulation results, compiled in Fig. (15), show that the overall path of the forces inside the rectangular lattices are directed to the down-left, whereas the path for the forces inside the triangular lattices move in circles. We see in these figures that the maximum force magnitudes in Fig. (15) compared to the forces in Figs. (10, 12, 13, and 14) are smaller by one or two orders. Hence, even if we were to amplify this force, we still cannot obtain negative forces.

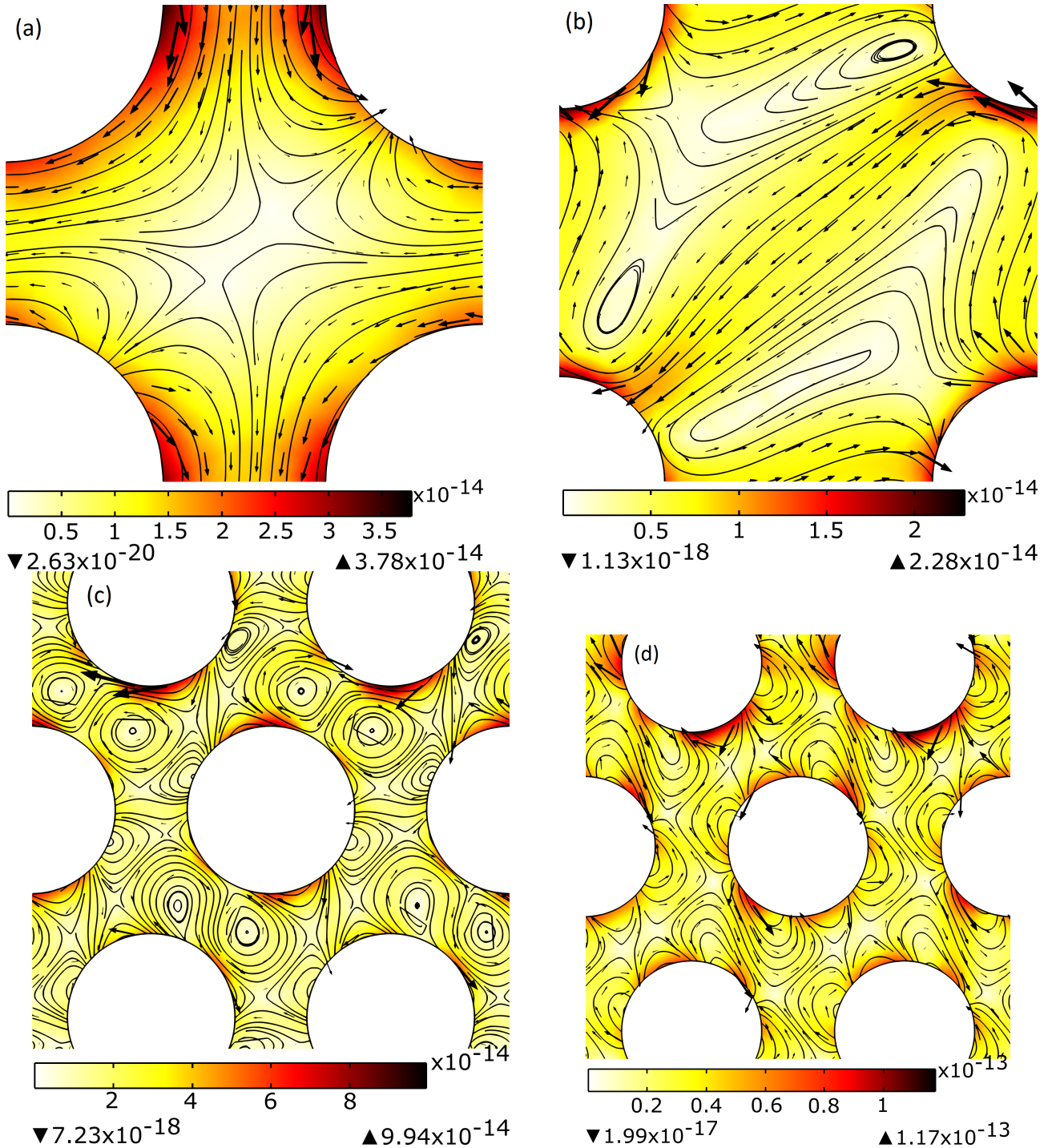


Figure 15. The force due to the curl of the field spin density. The color maps show the magnitude of the force; the arrows show the direction of the vector field and the streamlines show possible trajectories of the probe particle.

6. Conclusion

In this thesis, we have shown the non-trapping/scattering electromagnetic forces inside photonic crystals.

For the case of TM-polarized incident fields, the curl of the spin density is zero, hence the scattering forces only go in the direction of the Poynting vector. However, the power flow inside these crystals can only go in the positive direction, hence negative forces cannot arise in crystals with TM-polarized fields.

On the other hand, for the case of crystal structures with TE-polarized incident fields, we obtained forces that are not in the exact same direction of the power flow. However, the forces are moving in a direction reminiscent of negative refraction, but the vertical direction of the force remains positive.

References

1. Belov Pavel A., Hao Yang. Subwavelength Imaging at Optical Frequencies Using a Transmission Device Formed by a Periodic Layered Metal-Dielectric Structure Operating in the Canalization Regime. — 2006. — Vol. 73, no. 11.
2. Belov Pavel A., Simovski Constantin R., Ikonen Pekka. Canalization of Subwavelength Images by Electromagnetic Crystals. — 2005. — Vol. 71, no. 19.
3. Bogdanov Andrey A., Shalin Alexander S., Ginzburg Pavel. Optical Forces in Nanorod Metamaterial. — 2015. — Vol. 5. — P. 15846.
4. Brownian Motion in a Designer Force Field: Dynamical Effects of Negative Refraction on Nanoparticles / A. Cuche, B. Stein, A. Canaguier-Durand et al. — 2012. — Vol. 12, no. 8. — P. 4329–4332.
5. Derbali J., AbdelMalek F. Dual Negative Refraction in a Two Dimension Square Photonic Crystal. — 2015. — Vol. 350. — P. 213–216.
6. Draine B. T. The Discrete-Dipole Approximation and Its Application to Interstellar Graphite Grains. — 1988. — Vol. 333. — P. 848–872.
7. Engheta Nader, Ziolkowski R.W. A Positive Future for Double-Negative Metamaterials. — 2005. — Vol. 53, no. 4. — P. 1535–1556.
8. Foteinopoulou S., Economou E. N., Soukoulis C. M. Refraction in Media with a Negative Refractive Index. — 2003. — Vol. 90, no. 10.
9. Guide-Wave Photonic Pulling Force Using One-Way Photonic Chiral Edge States / Danlu Wang, Chengwei Qiu, Peter T. Rakich, Zheng Wang // CLEO: QELS_Fundamental Science. — Optical Society of America, 2015. — P. FM2D–7.

10. Hagemann H.-J., Gudat W., Kunz C. Optical Constants from the Far Infrared to the X-Ray Region: Mg, Al, Cu, Ag, Au, Bi, C, and Al₂O₃. — 1975. — Vol. 65, no. 6. — P. 742.
11. Jackson John David. Classical Electrodynamics. — 3rd edition. — Wiley, 1999.
12. Johnson Peter B., Christy R. W. Optical Constants of the Noble Metals. — 1972. — Vol. 6, no. 12. — P. 4370.
13. Kemp Brandon A., Kong Jin Au, Grzegorczyk Tomasz M. Reversal of Wave Momentum in Isotropic Left-Handed Media. — 2007. — Vol. 75, no. 5.
14. Magnetism from Conductors and Enhanced Nonlinear Phenomena / John B. Pendry, A. J. Holden, D. J. Robbins, W. J. Stewart. — 1999. — Vol. 47, no. 11. — P. 2075–2084.
15. Marqués Manuel I. Beam Configuration Proposal to Verify That Scattering Forces Come from the Orbital Part of the Poynting Vector. — 2014. — Vol. 39, no. 17. — P. 5122.
16. Moreno Ivan, Araiza J. Jesus, Avendano-Alejo Maximino. Thin-Film Spatial Filters. — 2005. — Vol. 30, no. 8. — P. 914–916.
17. Novotny Lukas, Hecht Bert. Principles of Nano-Optics. — Cambridge University Press, 2006.
18. Optical Constants of Electron-Beam Evaporated Boron Films in the 6.8–900 eV Photon Energy Range / Mónica Fernández-Perea, Juan I. Larruquert, José A. Aznárez et al. — 2007. — Vol. 24, no. 12. — P. 3800–3807.
19. Optical Pulling Force / Jun Chen, Jack Ng, Zhifang Lin, C. T. Chan. — 2011. — Vol. 5, no. 9. — P. 531–534.

20. Pendry John Brian. Negative Refraction Makes a Perfect Lens. — 2000. — Vol. 85, no. 18. — P. 3966.
21. Photonic Crystals: Molding the Flow of Light / John D. Joannopoulos, Steven G. Johnson, Joshua N. Winn, Robert D. Meade. — Princeton University Press, 2008.
22. Refraction and Rightness in Photonic Crystals / Rados Gajić, Ronald Meisels, Friedemar Kuchar, Kurt Hingerl. — 2005. — Vol. 13, no. 21. — P. 8596–8605.
23. Russell Phillip. Photonic Crystal Fibers // Frontiers in Optics (2003), Paper MO1. — Optical Society of America, 2003. — P. MO1.
24. Scattering Forces within a Left-Handed Photonic Crystal / Angeleene S. Ang, Sergey V. Sukhov, Aristide Dogariu, Alexander S. Shalin. — 2017. — Vol. 7. — P. 41014.
25. Shalaev Vladimir M. Optical Negative-Index Metamaterials. — 2007. — Vol. 1, no. 1. — P. 41–48.
26. Smith David R., Kroll Norman. Negative Refractive Index in Left-Handed Materials. — 2000. — Vol. 85, no. 14. — P. 2933.
27. Spectral Negative Refraction and Focusing Analysis of a Two-Dimensional Left-Handed Photonic Crystal Lens / K. Guven, K. Aydin, K. Alici et al. — 2004. — Vol. 70, no. 20.
28. Veselago Viktor G. The Electrodynamics of Substances with Simultaneously Negative Values of ε and μ . — 1968. — Vol. 10, no. 4. — P. 509–514.
29. Veselago Victor G. Energy, Linear Momentum and Mass Transfer by an Electromagnetic Wave in a Negative-Refraction Medium. — 2009. — Vol. 52, no. 6. — P. 649–654.

30. Yannopapas Vassilios, Galiatsatos Pavlos G. Electromagnetic Forces in Negative-
Refractive-Index Metamaterials: A First-Principles Study. — 2008. — Vol. 77, no. 4.